Journal Pre-proof

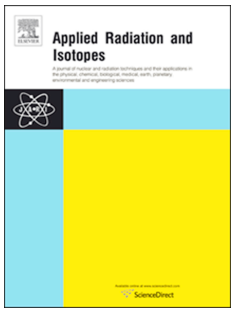

Impact of high energy photons on physical, structural and magnetic properties of $Mn_{0.65}Zn_{0.35}Fe_{2-x}Nd_xO_4$ nanoparticles

Pranav P. Naik, Sher Singh Meena, Pramod Bhatt, Diptesh Naik, Rahul Singhal

PII: S0969-8043(23)00465-7

DOI: https://doi.org/10.1016/j.apradiso.2023.111112

Reference: ARI 111112

To appear in: *Applied Radiation and Isotopes*

Received Date: 14 July 2023

Revised Date: 19 October 2023

Accepted Date: 11 November 2023

Please cite this article as: Naik, P.P., Meena, S.S., Bhatt, P., Naik, D., Singhal, R., Impact of high energy photons on physical, structural and magnetic properties of $Mn_{0.65}Zn_{0.35}Fe_{2-x}Nd_xO_4$ nanoparticles, *Applied Radiation and Isotopes* (2023), doi: https://doi.org/10.1016/j.apradiso.2023.111112.

This is a PDF file of an article that has undergone enhancements after acceptance, such as the addition of a cover page and metadata, and formatting for readability, but it is not yet the definitive version of record. This version will undergo additional copyediting, typesetting and review before it is published in its final form, but we are providing this version to give early visibility of the article. Please note that, during the production process, errors may be discovered which could affect the content, and all legal disclaimers that apply to the journal pertain.

© 2023 Published by Elsevier Ltd.

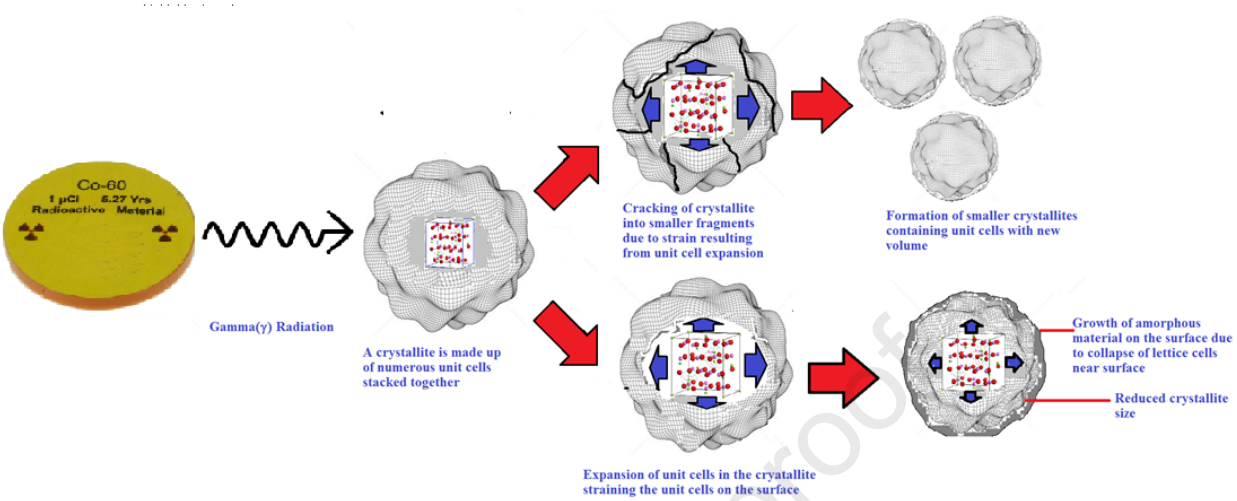

MODEL FOR EFFECT OF GAMMA RADIATION ON $Mn_{0.65}Zn_{0.35}Fe_{2-x}Nd_xO_4$ NANOPARTICLES

Journal Pre-proof

Journal Pre-proof

Impact of High Energy Photons on Physical, Structural and Magnetic properties of $Mn_{0.65}Zn_{0.35}Fe_{2-x}Nd_xO_4$ Nanoparticles

Pranav P. Naik[1,*], Sher Singh Meena[2], Pramod Bhatt[2], Diptesh Naik[3] Rahul Singhal[4]
[1]School of Physical and Applied Sciences, Goa University, Taleigao Plateau - Goa 403206
[2]Solid State Physics Division, Bhabha Atomic Research Centre, Mumbai, Maharashtra 400085, India.
[3]School of Chemical Sciences, , Goa University, Taleigao Plateau - Goa 403206
[4]Department of Physics, Malaviya National Institute of Technology, Jaipur, Rajasthan 302017,India
*Email: pranav.naik@unigoa.ac.in

Abstract: Ultrafine powders of Nd^{+3} doped Mn-Zn ferrite powders with composition $Mn_{0.65}Zn_{0.35}Fe_{2-x}Nd_xO_4$ (x=0.04, 0.06, 0.08) were prepared using combustion method of preparation. Monophasic nanoparticle formation was confirmed by X-ray diffraction. The particle size was determinedusing Transmission electron microscope (TEM). The nanopowders were investigated for their physical, structural and magnetic properties and then radiated with gamma photons obtained from Co^{60} source with a dose of 500Gy, 750Gy and 1000Gy. The characterization of radiated powders showed preservation of spinel structure with breaking down of crystallites into finer crystals with increment in amorphous content. Structural and physical parameters were drastically altered due to high energy photon exposure. The breaking down of larger particles was observed as a result of photon energy impact on the samples. The Saturation magnetization of ferrite nanoparticles was observed to increase with increasing gamma radiation dose. Mössbaure spectra showed the dominance of Fe^{+3} in the high spin state.

Keywords: Ferrite; gamma radiation exposure; particle size; Mössbauer spectroscopy.

1. Introduction

Manganese zinc ferrite belongs to a family of magnetic ceramics with general formula AB_2O_4 (A-divalent metal ion, B-trivalent metal ion:generally Fe) that finds applications in the production of several electronic components [1-5]. These materials are known for their highly useful magnetic properties, like low loss hysteresis, single domain materials, superparamagnetic behavior, a large value of initial permeability, incomparably low eddy currents due to high room temperature resistivity and low dielectric losses, etc. They stand as potential candidates for application of modern eras such as microwave devices, electromagnetic interference suppressors (EMIS), different types of sensors including medical sensor applications, targeted drug delivery systems, hyperthermia, ferrofluids, heat transfer applications in nuclear reactors and several other applications [1]. These unique properties of manganese zinc ferrites are governed by several parameters one being the cations occupying the tetrahedral sites and the octahedral sites present in the ferrite lattice. One can alter the properties by altering the cation distribution at these two sites [2]. According to several reports, the inclusion of rare earth at the octahedral site in the ferrite structure can alter the structural, magnetic,

and electrical properties of the ferrite nanomaterials to a substantial magnitude [3,4,5]. Such doping results in the coupling of 4f electrons of rare earth ions and 3d electrons of transition elements causing alterations in the magnetic and electrical properties of ferrite material. However, the task of rare earth doping is also associated with difficulties such as limited solubility of rare earth ions in the ferrite structure. This difficulty is partially overcome by including lower concentrations of rare earth material in the host matrix [6]. As per the available reports, a significant variation in cation distribution can be achieved by exposing nanoparticle ferrite material to high-energy gamma radiation photons. It has been shown that high energy photon interaction with nanoparticle ferrite material can produce cognizable modifications in various properties of the material [7, 8-13]. In our previous work, we have elaborated on the impact of rare earth doping and gamma radiation exposure on the structural and electrical properties of $Mn_{0.65}Zn_{0.35}Fe_{2-x}Nd_xO_4$ (x = 0.04, 0.05, and 0.06). In the present research report, interesting findings on magnetic alterations observed in high energy photon radiated $Mn_{0.65}Zn_{0.35}Fe_{2-x}Nd_xO_4$ (x = 0.04, 0.06, and 0.08) are reported and explained on the basis of a stress model that has never been proposed earlier.

2. Experimental

Ferrite powders with composition $Mn_{0.65}Zn_{0.35}Fe_{2-x}Nd_xO_4$ (x = 0.04, 0.06, and 0.08) were prepared using the combustion route [7,8,15-20]. The acetates and nitrates of the metal ions were taken in stoichiometric proportion along with Nitrilotriacetic acid (NTA) and Glycine. A clear solution was obtained by dissolving all the reactants in the double distilled water at 80^{o}C. This solution was further subjected to volume reduction by continuous heating to obtain a dry mass that undergoes combustion once the ignition temperature is reached. The residual product obtained after the combustion of dry mass was crushed into a fine powder and used for characterization and study of various investigations. The characterized powdered samples were pressed into pellets (diameter=10 mm, thickness = 2.5 mm). Three sets of pallets were exposed to three different doses of γ radiation. The γ radiations of wavelengths λ=0.0106 Å with energy E_1 = 1.17MeV and wavelength λ = 0.009 Å with energy E_2 = 1.33MeV obtained from ^{60}Co source were used to irradiate these samples for different pre-calculated time durations in order to obtain the radiation dose of 500Gy, 750Gy and 1000Gy. Gamma irradiated samples were further characterized using X-ray diffraction (XRD) using Rigaku X-Ray diffractometer (Cu Kα, λ=1.5418Å) for investigating structural alterations if any. Transmission electron micrographs were obtained on a transmission electron microscope(TEM) (Model and make: FEI Tecnai G2, F30, IIT Bombay, India) to investigate the variation in the particle size both prior to radiation exposure and after the exposure. Physical, Structural, and magnetic properties of as-prepared and irradiated samples were investigated using appropriate experimental techniques.

Magnetic hysteresis loops were obtained using Quantum Design's Versa Lab 3T vibrating sample magnetometer (VSM). Mössbauer spectra measurements and analysis were also carried out using a conventional Mössbauer spectrometer in constant acceleration mode with Co-57 radioactive source embedded in a rhodium matrix of 50 mCi (BARC, Mumbai, India). The observed variations in the properties that have been investigated are being supported with a suitable stress model.

3. Results & discussion

3.1 X-Ray diffraction

The Rietveld refined X-ray diffraction patterns of as-prepared (Nd+3) doped Manganese Zinc ferrite powders with composition $Mn_{0.65}Zn_{0.35}Fe_{2-x}Nd_xO_4$ (x = 0.04, 0.06 and 0.08) were obtained on Rigaku X-Ray diffractometer (Cu Kα, λ=1.5418Å) and are presented in Figure 1. The Rietveld refined XRD patterns obtained on high energy gamma photon radiated $Mn_{0.65}Zn_{0.35}Fe_{1.92}Nd_{0.08}O_4$ with different radiation doses are presented in Figure 2 which confirmed the formation of monophasic cubic spinel structure. The values of lattice constant '*a*', mass density, Crystallite size't', porosity (%), R_{wp}, $R_{exp,}$ and χ^2 for as-prepared and high energy gamma photon irradiated $Mn_{0.65}Zn_{0.35}Fe_{2-x}Nd_xO_4$ nanopowders are presented in Table 1.

Journal Pre-proof

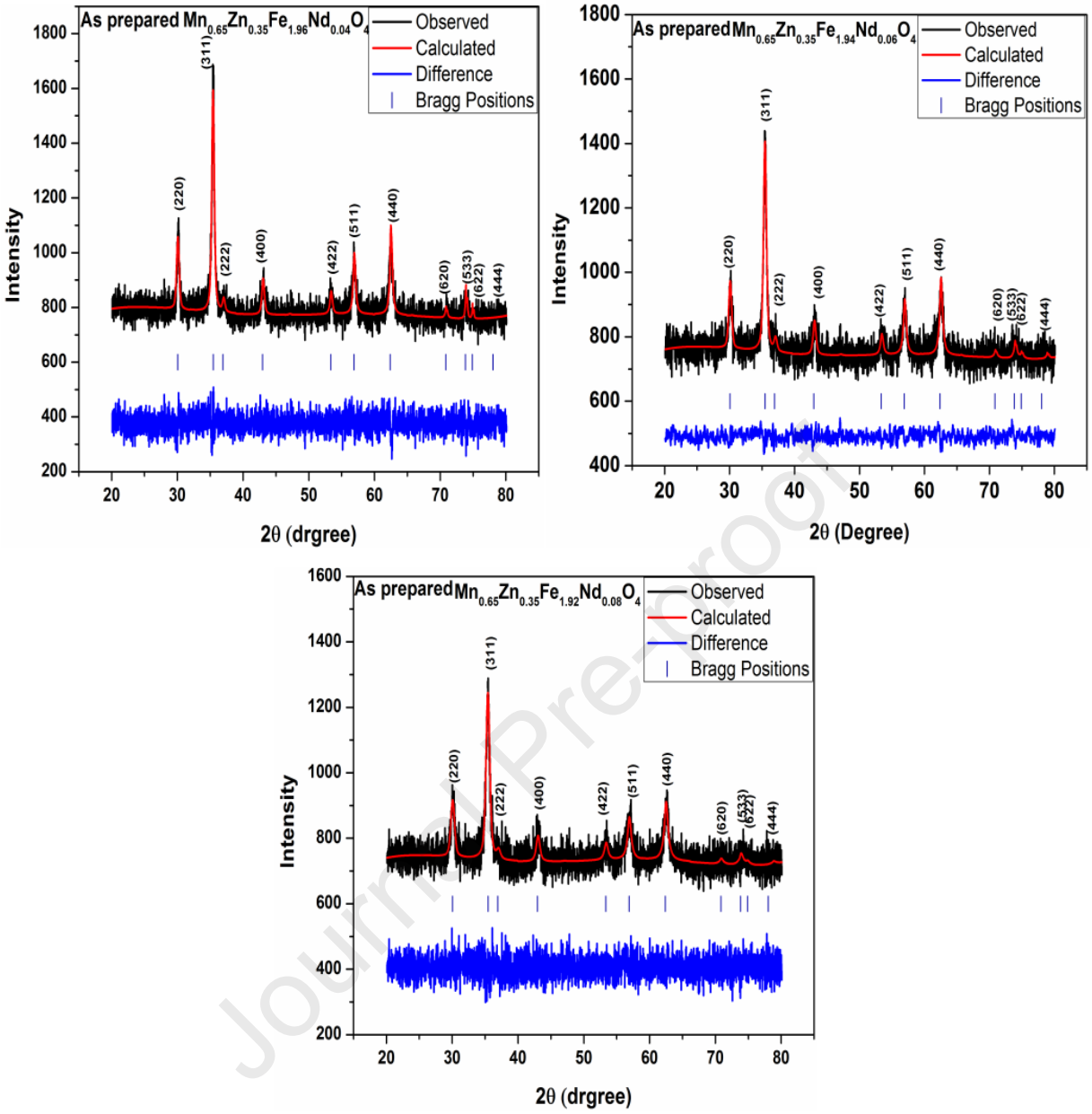

Figure 1 X-ray diffraction patterns obtained on as-prapared $Mn_{0.65}Zn_{0.35}Fe_{2-x}Nd_xO_4$ nanoparticles

Journal Pre-proof

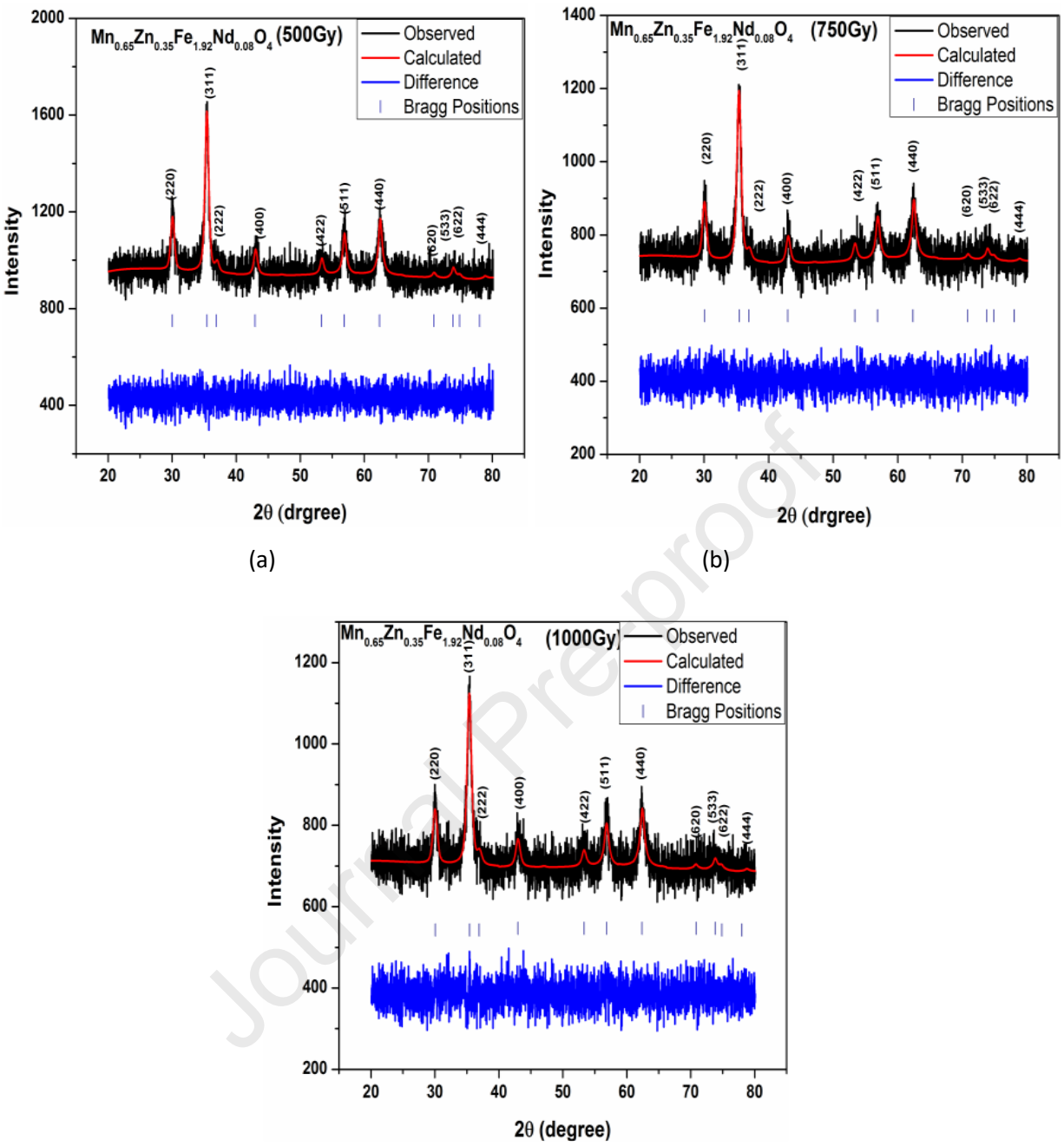

Figure 2 Rietveld refined XRD patterns of high energy gamma photon radiated $Mn_{0.65}Zn_{0.35}Fe_{1.96}Nd_{0.08}O_4$ irradiated with (a) 500Gy (b) 750Gy (c) 1000Gy

Here Rwp, Rexp, and χ^2 are the discrepancy factor, expected value, and the goodness fit factor respectively. The X-ray diffraction patterns were fitted with the Fd3m space group assigning the tetrahedral ions at 8a sites while the octahedral ions were assigned 16d sites. The samples were seen to retain the original spinel structure even after gamma irradiation without the formation of any secondary phase.

Table 1 Variation of lattice constant '*a*', mass density, Crystallite size 't', porosity, Rwp, Rexp and χ^2 for as-prepared and gamma irradiated $Mn_{0.65}Zn_{0.35}Fe_{2-x}Nd_xO_4$ nanopowders

'Nd^{+3}' Concentration (x)	Gamma radiation Dose (Gy)	Lattice constant '*a*' Å	Mass Density 'D_M' (g/cc)	Crystallite Size 't' (nm)	Porosity (%)	R_{WP}	R_{EXP}	χ^2
0.04	0Gy	8.432(8)	3.34(3)	18±3	36.68	19.19	14.32	1.34
	500Gy	8.433(9)	3.30(6)	15±3	37.35	18.3	14.52	1.26
	750Gy	8.435(2)	3.20(7)	12±2	39.21	16.31	12.64	1.29
	1000Gy	8.436(1)	3.17(2)	10±2	39.85	18.35	12.92	1.42
0.06	0Gy	8.435(4)	3.48(6)	16±2	34.42	21.01	14.39	1.46
	500Gy	8.436(8)	3.51(7)	14±3	35.69	18.35	13.49	1.36
	750Gy	8.438(2)	3.41(2)	11±1	37.59	19.37	13.64	1.42
	1000Gy	8.439(4)	3.40(5)	10±2	37.70	20.31	15.21	1.55
0.08	0Gy	8.441(4)	3.55(7)	15±3	33.46	20.86	15.01	1.39
	500Gy	8.441(9)	3.51(7)	13±2	34.18	20.34	15.18	1.34
	750Gy	8.442(5)	3.41(2)	11±3	36.13	21.12	14.17	1.49
	1000Gy	8.442(7)	3.40(5)	10±2	36.25	20.24	13.05	1.56

Table 2 Variation of FWHM $_{(311)}$, lattice strain, and crystallite size with gamma radiation dose for as-prepared and gamma irradiated $Mn_{0.65}Zn_{0.35}Fe_{2-x}Nd_xO_4$ nanopowders

'Nd^{+3}' Concentration (x)	Gamma radiation Dose (Gy)	$FWHM_{(311)}$ In radians	Lattice Strain 'ε'	Crystallite Size 't' (nm)
0.04	0Gy	0.0081	0.0064	18±3
	500Gy	0.0097	0.0077	15±3
	750Gy	0.0121	0.0096	12±2
	1000Gy	0.0145	0.0116	10±2
0.06	0Gy	0.0091	0.0072	16±2
	500Gy	0.0104	0.0083	14±3
	750Gy	0.0132	0.0105	11±1

Journal Pre-proof

	1000Gy	0.0145	0.0116	10±2
0.08	0Gy	0.0091	0.0072	15±3
	500Gy	0.0104	0.0083	13±2
	750Gy	0.0132	0.0105	11±3
	1000Gy	0.0145	0.0115	10±2

However, a substantial decrease in diffraction peak intensities accompanied by their broadening depicted by FWHM values listed in 2 indicated lowering of crystalline nature and reduction of crystallite sizes in the samples. The amorphous character introduced in the material was found to increase with increasing gamma radiation dose. This phenomenon of crystallite size reduction and introduction of partial amorphous nature can be explained on the bases of a strain-based model which is presented in Figure 3.

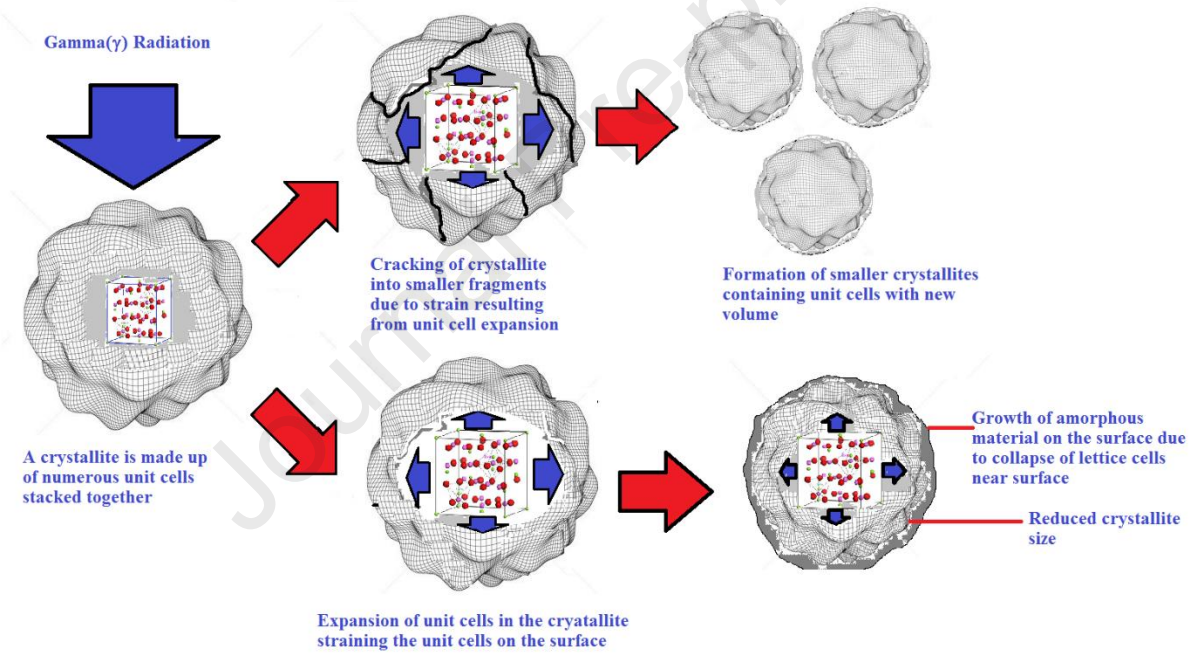

Figure 3 Hypothetical model for reduction of crystallite size

The decrease in crystallite size of all the samples, decrease in the intensity of all XRD peaks, increase in lattice constant (Table 1), and increase in bond lengths after their exposure to high energy photons, as seen from Table 3, 4 5 and 6, provides adequate evidence to vouch on the fact that this is just impossible unless there is an increase of amorphous content in the material as a consequence of the tremendous stress developed in the crystallites after their exposure to high energy photons.

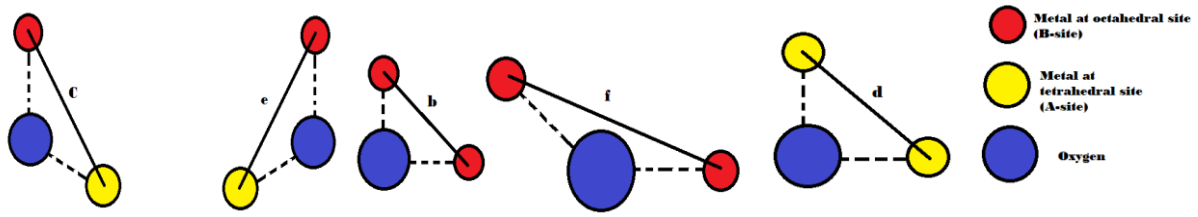

A-B interaction B-B interaction A-A interaction

Figure 4 Ion pair configuration in ferrite with bond lengths between the cations

Various ion pair configurations and bond lengths between the cations resulting in different interactions in ferrite lattice are shown in Figure 4 [8].

Table 3 Variation of bond lengths between cations for $Mn_{0.65}Zn_{0.35}Fe_{2-x}Nd_xO_4$

Sample $Mn_{0.65}Zn_{0.35}Fe_{2-x}Nd_xO_4$	*b* (Å)	*c* (Å)	*d* (Å)	*e* (Å)	*f* (Å)
x=0.04	2.979(1)	3.493(3)	3.648(6)	5.472(9)	5.159(9)
x=0.06	2.979(6)	3.493(9)	3.649(3)	5.473(9)	5.160(9)
x=0.08	2.981(4)	3.495(9)	3.651(4)	5.477(1)	5.163(8)

Table 4 Variation of bond lengths between cations for $Mn_{0.65}Zn_{0.35}Fe_{2-x}Nd_xO_4$ irradiated with 500Gy

Sample $Mn_{0.65}Zn_{0.35}Fe_{2-x}Nd_xO_4$	*b* (Å)	*c* (Å)	*d* (Å)	*e* (Å)	*f* (Å)
x=0.04	2.979(3)	3.493(6)	3.649(1)	5.473(5)	5.160(4)
x=0.06	2.980(2)	3.494(6)	3.650(1)	5.475(1)	5.161(9)
x=0.08	2.981(5)	3.496(1)	3.651(6)	5.477(4)	5.164(2)

Table 5 Variation of bond lengths between cations for $Mn_{0.65}Zn_{0.35}Fe_{2-x}Nd_xO_4$ irradiated with 750Gy

Sample $Mn_{0.65}Zn_{0.35}Fe_{2-x}Nd_xO_4$	*b* (Å)	*c* (Å)	*d* (Å)	*e* (Å)	*f* (Å)
x=0.04	2.979(7)	3.494(1)	3.649(5)	5.474(2)	5.161(1)
x=0.06	2.980(6)	3.495(1)	3.650(5)	5.475(8)	5.162(6)
x=0.08	2.981(8)	3.496(4)	3.651(9)	5.477(9)	5.164(6)

Table 6 Variation of bond lengths between cations for $Mn_{0.65}Zn_{0.35}Fe_{2-x}Nd_xO_4$ irradiated with 1000Gy

Sample $Mn_{0.65}Zn_{0.35}Fe_{2-x}Nd_xO_4$	*b* (Å)	*c* (Å)	*d* (Å)	*e* (Å)	*f* (Å)
x=0.04	2.980(2)	3.494(6)	3.650(1)	5.475(1)	5.161(9)
x=0.06	2.980(9)	3.495(4)	3.650(8)	5.476(3)	5.163(1)
x=0.08	2.982(1)	3.496(8)	3.652(3)	5.478(4)	5.165(1)

The empirical understanding of these observations and conclusions can passably be provided by proposing a model as given in Figure 3. The effect of including Nd^{+3} with ionic radius 1.12 Å in the material is limited to minor enhancement of lattice constant as far as structural change is concerned however it has effects of lager magnitude on other properties like magnetic and electrical properties. But these variations appear to be shielded by further improvements in the variations brought about by the high energy photon dose given to the samples. Exposure of nanoparticle material to high energy photons takes Fe^{+2} along with Fe^{+3} which is a major component in the material on both the tetrahedral and the octahedral sites [9] as compared to Fe^{+2} in the high spin state, both of which have larger ionic radii which vary between 0.72Å to 0.74Å respectively. The increase in ionic radii develops additional frustration in the crystallite on account of increased stress within the crystallites. The increased stress is marginally compensated by an increase in lattice constant and the bond lengths. This increment in the lattice constant results in an increase in the unit cell volume within the entire crystallite. This increase that simultaneously occurs and increases with an increase in the radiation dose develops a large amount of pressure within the crystallite. Thus a stage is reached when the stress developed within the crystal due to high energy received from the photon overwhelms the bonding adjustments in certain sections of the crystal. The increased pressure within the entire crystallite can produce two types of effects. Firstly the pressure build-up within the crystals can break the larger crystallites into smaller crystals thereby increasing the surface area of the material, the porosity of the material with a proportionate decrease in the material density. Secondly, the effect of pressure pushes the unit cells near the surface into a disordered structure as these are in an unbalanced environment with no appropriate bonding at the surface. Since this would occur at all crystallite surfaces it results in an increase of the amorphous component in the sample. Applying the same analogy to all the crystallites in the samples would show a drastic decrement in average crystallite

size, and mass density with an appropriate increase in amorphous content and sample porosity. This particular character would increase with increasing radiation dose [17-19].

3.2. Transmission electron microscopy

Figure 5 shows transmission electron micrographs and the particle size distribution histograms obtained for as-prepared and gamma irradiated $Mn_{0.65}Zn_{0.35}Fe_{1.96}Nd_{0.04}O_4$ nanoparticles. The values of particle size estimated from transmission electron micrographs for as-prepared and gamma irradiated samples are listed in Table 7.

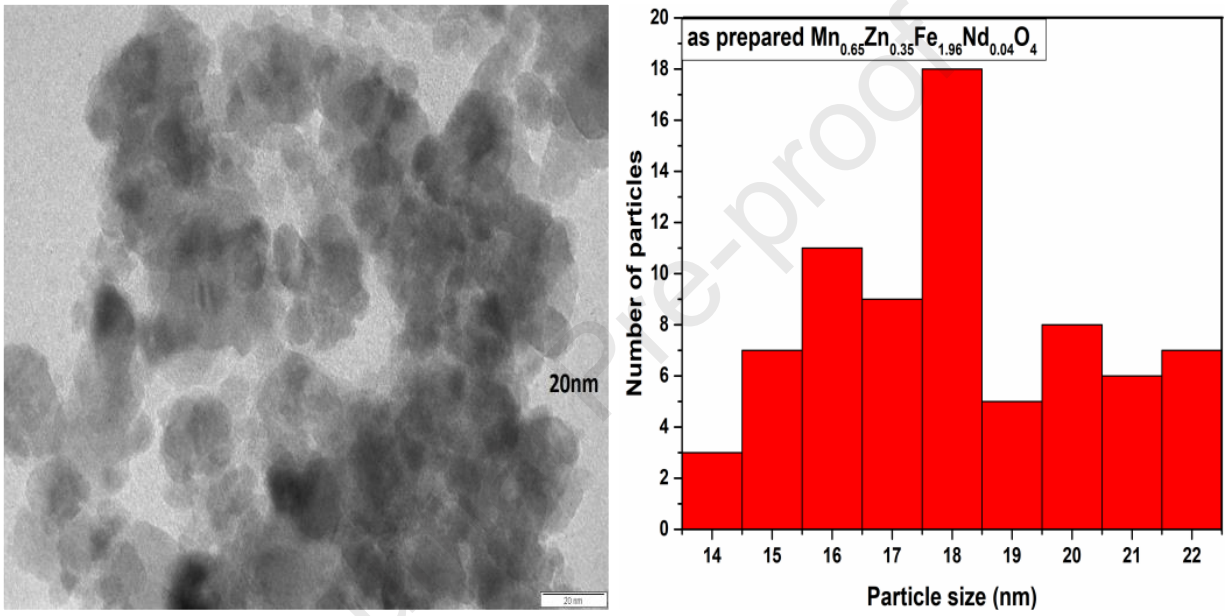

(a)

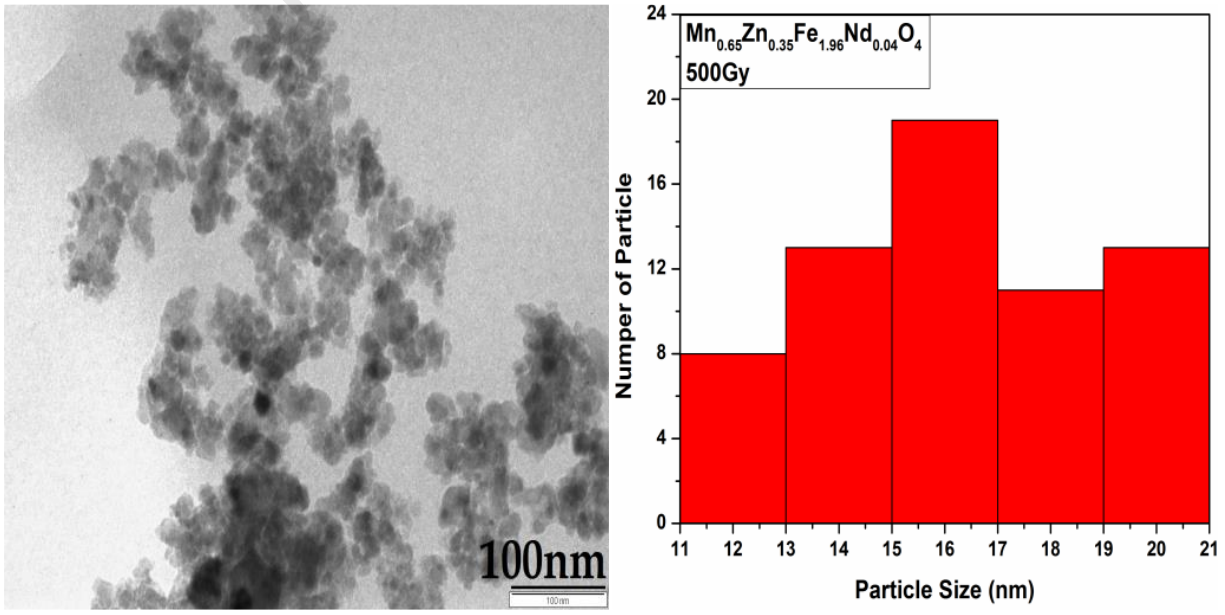

(b)

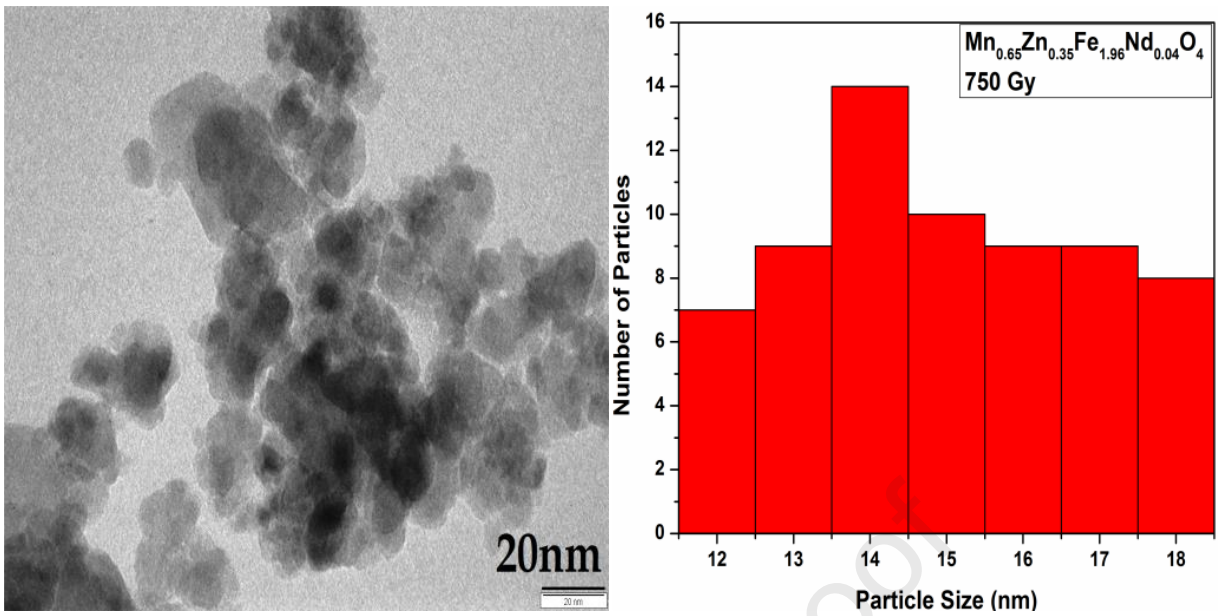

(c)

Figure 5 Transmission electron micrographs and the particle size distribution histograms of asprepared and gamma irradiated $Mn_{0.65}Zn_{0.35}Fe_{2-x}Nd_xO_4$

Table 7 Variation of particle size with Nd^{+3} concentrations for gamma irradiated $Mn_{0.65}Zn_{0.35}Fe_{2-x}Nd_4O_4$

Concentration Of Nd^{+3} 'x'	As-prapared Particle Size (nm)	500Gy Particle Size (nm)	750Gy Particle Size (nm)	1000Gy Particle Size (nm)
0.04	20±4	16±4	14±4	12±3
0.06	18±2	15±3	13±3	11±3
0.08	18±3	15±3	15±3	12±3

The micrographs and the particle size histograms showed an enhancement in the ranges of particle size as well as in the number of particles of various sizes. This may be attributed to the fact that there is a cracking of larger particles into smaller particles due to the internal crystalline strain that is developed due to an increase in the lattice size and unit volume size as a result of gamma radiation. This also supports the fact that the crystalline strain increases with increasing gamma radiation dose thereby breaking bigger particles into smaller ones with the development of disorder or amorphous material in small amounts. In the case of smaller particles, the stress developed within the crystallites may not be sufficient for fragmentation of the particle and would result in the production of amorphous material near the surface due to differences in the environment. The theme sustaining the

proposed model that is strongly supported by other parameters like density, porosity, crystallite size, etc. seems to find constructive support from TEM as well, as, an increase in the population of particles of lower size is seen in the micrographs [21-24].

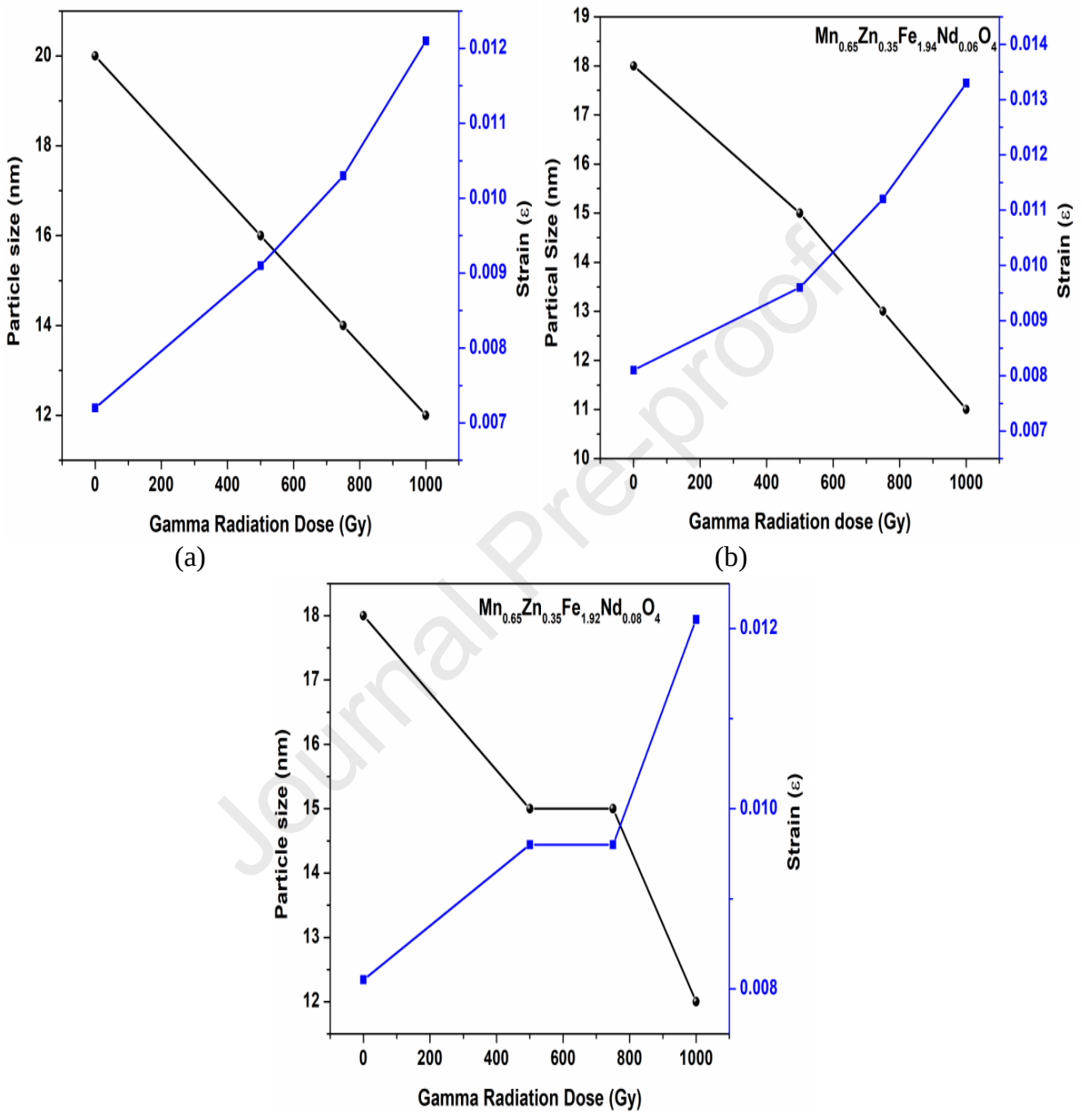

Figure 6 Variation particle strain and particle size with gamma radiation dose for $Mn_{0.65}Zn_{0.35}Fe_{2-x}Nd_xO_4$

Figure 6 shows the effect of gamma radiation on the strain as well as particle size in the radiated samples that support the analogy formulation in the proposed model.

3.4 Magnetic properties

The comparative Magnetic hysteresis loops obtained for as-prepared and gamma-irradiated $Mn_{0.65}Zn_{0.35}Fe_{2-x}Nd_xO_4$ nanoparticles irradiated with 500Gy, 750Gy and 1000Gy obtained on VSM are shown in Figure 7 and the squareness ratios (M_R/M_S) for all the samples are listed in Table 8.

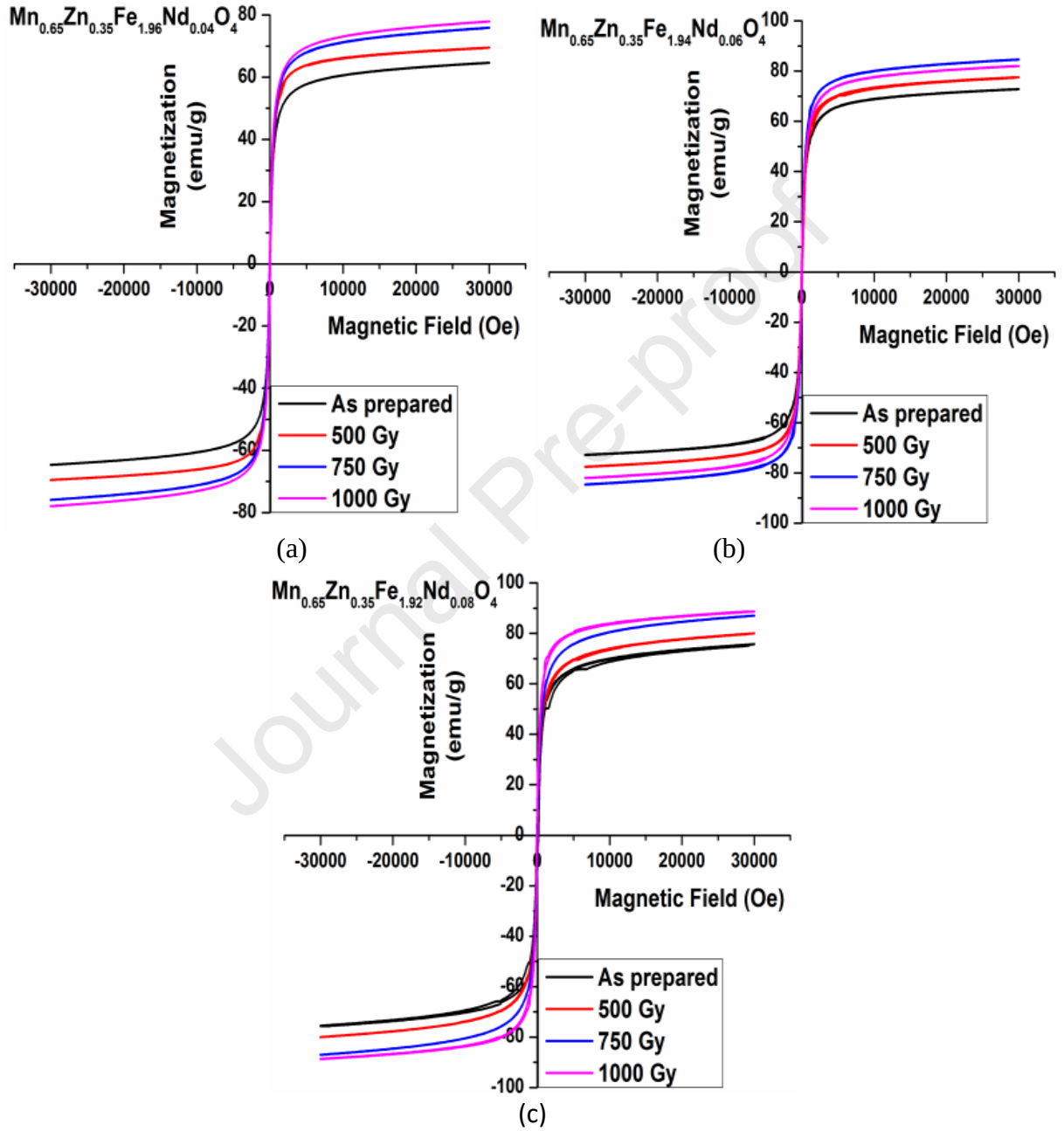

Figure 7 Hysteresis curves of as-prepared and gamma irradiated $Mn_{0.65}Zn_{0.35}Fe_{2-x}Nd_xO_4$ nanoparticles

All the samples were seen to exhibit negligible hysteresis loss indicating superparamagnetic behavior which could be also inferred from low squareness values for all, as-prepared and gamma-irradiated

samples. Saturation magnetization for as-prepared samples was seen to increase as discussed in our previous reports [8,22-23]

Table 8 Squareness ratio (M_R/M_S) for as-prepared and gamma irradiated $Mn_{0.65}Zn_{0.35}Fe_{2-x}Nd_xO_4$ nanoparticles

Nd^{+3} concentrations 'x'	M_R/M_S Ratio for 500 Gy	M_R/M_S Ratio for 500 Gy	M_R/M_S Ratio for 750 Gy	M_R/M_S Ratio for 1000 Gy
0.04	0.032	0.011	0.009	0.007
0.06	0.019	0.010	0.008	0.008
0.08	0.020	0.010	0.009	0.008

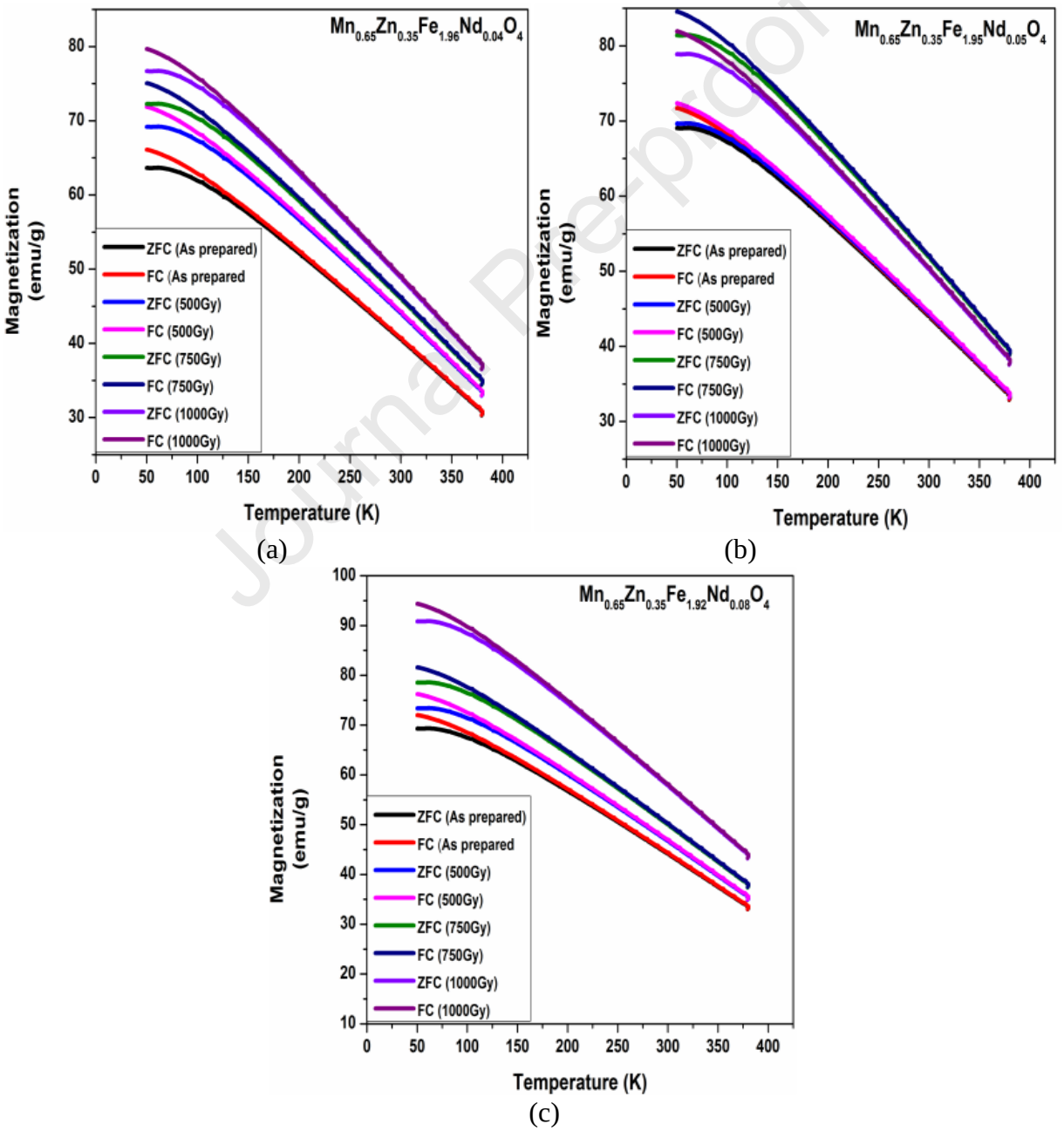

(a) (b)

(c)

Journal Pre-proof

Figure 8 Field cooled (FC) and zero field cooled (ZFC) curves for as-prapared and gamma irradiated $Mn_{0.65}Zn_{0.35}Fe_{2-x}Nd_xO_4$ nanoparticles

Table 9 Variation of T_{MAX} and T_{DIFF} obtained for gamma irradiated $Mn_{0.65}Zn_{0.35}Fe_{2-x}Nd_xO_4$ nanoparticles

Nd^{+3} concentration 'x'	As-prapared		500Gy		750Gy		1000Gy	
	T_{MAX} (K)	T_{DIFF} (K)	T_{MAX} (K)	T_{DIFF} (K)	T_{MAX} (K)	T_{DIFF} (K)	T_{MAX} (K)	T_{DIFF} (K)
0.04	71	121	71	120	68	119	66	118
0.06	70	119	67	118	66	117	64	117
0.08	68	118	67	118	63	117	62	116

Variation of magnetization as a function of temperature was determined for as-prepared and gamma-irradiated $Mn_{0.65}Zn_{0.35}Fe_{2-x}Nd_xO_4$ nanoparticles over the temperature range of 50K to 385K at a constant applied field of 750Oe. The field-cooled (FC) and zero-field cooled (ZFC) curves obtained for γ irradiated samples are shown in Figure 8.

It was observed that the magnetization of samples increases with increasing gamma radiation dose. This increase in magnetization with increasing γ radiation dose can be attributed to increased concentrations of Fe^{+3} ions in high spin state at both tetrahedral sites and the octahedral sites which enhances the magnetic moment.

In order to understand the variation of blocking temperature with the particle size distribution, we define two temperatures T_{MAX} and $T_{DIFF.}$ Temperature T_{MAX} is taken as the blocking temperature of the smallest particles in the material while the T_{DIFF} is the blocking temperature of the larger particles in the samples.

It can be seen from table 9 that the temperature difference between T_{MAX} and T_{DIFF} is small for all samples. This difference actually gives the variation of blocking temperature for particles of various sizes in the material. A narrow temperature bandwidth is an indicator of the fact that particle size distribution in the samples is essentially small this is also evident from the particle size histograms obtained from TEM micrographs. The blocking temperature does not show any remarkable variation with increasing gamma radiation dose. For temperature below T_{MAX} which is the lowest blocking temperature, the magnetization remains constant which can be attributed to enhancing anisotropy due to stronger interparticle interactions, making moments pinned to one another with the thermal energy becoming smaller to overcome the energy barriers. The magnetization of field cooled curves was seen to increase further below T_{MAX} which can be attributed to better magnetic ordering and enhanced

magnetic character due to the dominance of Fe^{+3} ions in high spin state at both the octahedral and the tetrahedral sites in gamma irradiated samples. The magnetization curves for all gamma irradiated samples were observed to follow a decreasing trend for $T>T_{MAX}=T_B$ the blocking temperature obeying the Curie-Weiss law. The furcation observed in ZFC and FC plots beyond a particular temperature T_{DIFF} is indeed a characteristic observed in systems or samples containing superparamagnetic grains. It may be seen that similar behavior is observed in the plots obtained for all the samples. This fact suggests that the samples are made up of superparamagnetic grains which could be a single domain or a mixture of single domain and a small fraction of multidomain grains [28-32].

3.5 Mossbauer spectroscopy

Figure 9 shows Mössbauer spectra of as-prepared and gamma irradiated $Mn_{0.65}Zn_{0.35}Fe_{1.94}Nd_{0.06}O_4$ nanoparticles recorded at room temperature in the velocity of ±11.5 mm/s using conventional Mössbauer spectrometer. Mössbauer spectra for the samples were also fitted with three sextets and a paramagnetic doublet. The presence of these sextets can be attributed to superexchange interaction between the magnetic ions at A– and B–sub-lattices.

Journal Pre-proof

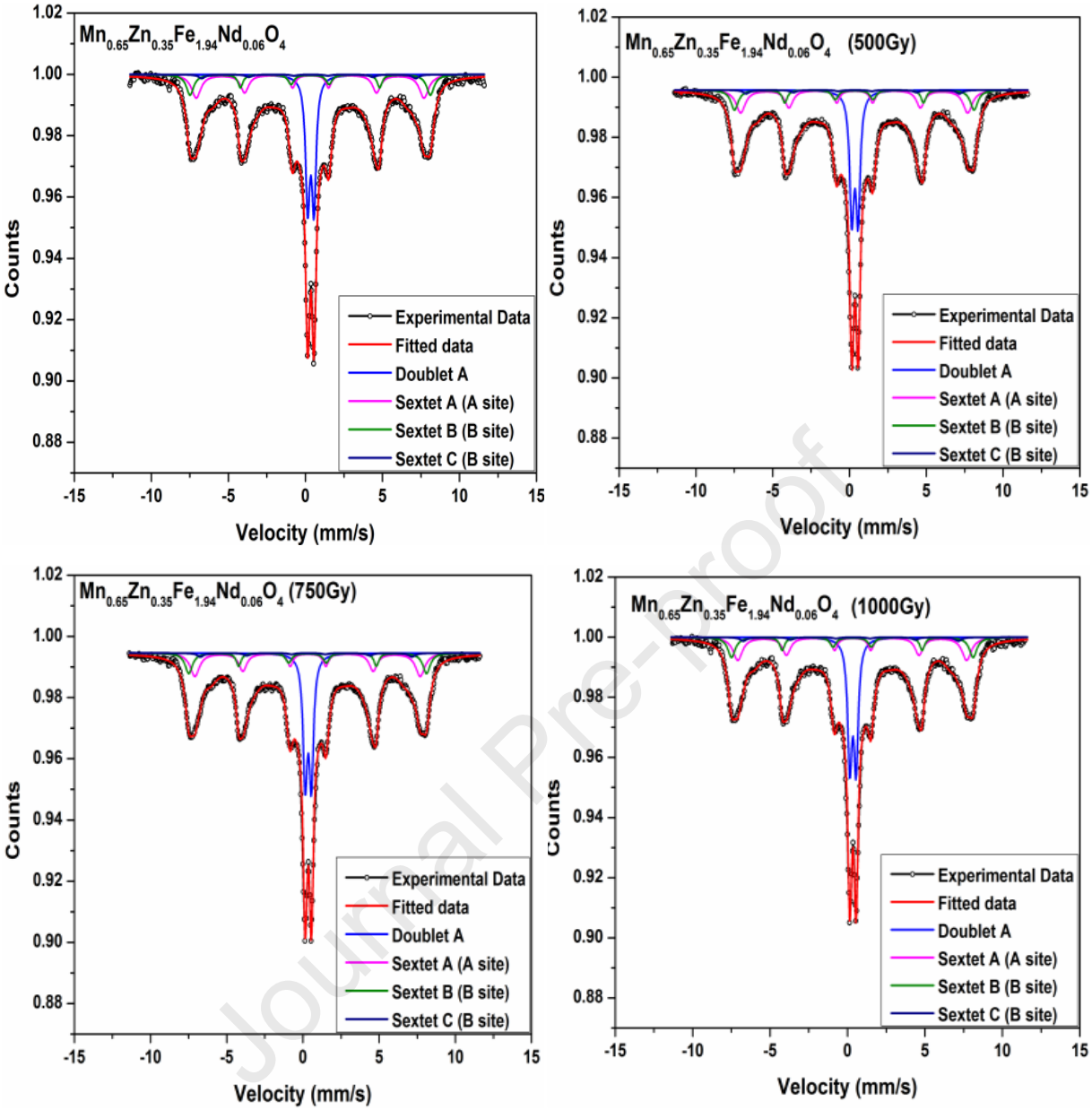

Figure 9 Mossbauer spectra for as-prepared and gamma irradiated $Mn_{0.65}Zn_{0.35}Fe_{2-x}Nd_xO_4$ nanoparticles

Table 10 Calculated values of isomer shift (IS), quadrupole splitting (QS) and hyperfine magnetic field for $Mn_{0.65}Zn_{0.25}Fe_{2-x}Nd_xO_4$ irradiated with 500Gy.

Sample	Iron site spectra	Isomer shift (IS) mm/s	Quadrupole splitting (QS) mm/s	Hyperfine field (Tesla)	Relative area (%)
X=0.04	Doublet (S. P.)	0.342±0.015	0.389±0.016	-	37.69

	Sextet A (Octa)	0.388±0.008	0.023±0.023	48.63±1.26	18.35
	Sextet B (Octa)	0.392±0.036	0.053±0.031	45.25±1.03	18.52
	Sextet C (Tetra)	0.292±0.016	0.042±0.016	36.96±1.36	25.97
X=0.06	Doublet (S. P.)	0.351±0.019	0.438±0.018	-	38.19
	Sextet A (Octa)	0.346±0.065	0.053±0.018	48.59±1.39	19.75
	Sextet B (Octa)	0.318±0.061	0.053±0.019	46.36±1.36	18.66
	Sextet C (Tetra)	0.286±0.009	0.036±0.015	36.35±0.09	23.41
X=0.08	Doublet (S. P.)	0.363±0.037	0.459±0.009	-	38.67
	Sextet A (Octa)	0.346±0.086	0.062±0.016	49.36±2.36	19.26
	Sextet B (Octa)	0.362±0.053	0.046±0.026	44.36±1.25	19.37
	Sextet C (Tetra)	0.299±0.021	0.038±0.011	33.16±2.56	22.70

Table 11 Calculated values of isomer shift (IS), quadrupole splitting (QS) and hyperfine magnetic field for $Mn_{0.65}Zn_{0.25}Fe_{2-x}Nd_xO_4$ irradiated with 750Gy.

Sample	Iron site spectra	Isomer shift (IS) mm/s	Quadrupole splitting (QS) mm/s	Hyperfine field (Tesla)	Relative area (%)
X=0.04	Doublet (S. P.)	0.353±0.011	0.435±0.011	-	37.98
	Sextet A (Octa)	0.386±0.025	0.068±0.009	48.83±2.36	19.25
	Sextet B (Octa)	0.328±0.026	0.046±0.028	45.23±1.39	19.36
	Sextet C (Tetra)	0.228±0.016	0.037±0.013	37.26±2.11	24.01
X=0.06	Doublet (S. P.)	0.359±0.035	0.426±0.045	-	38.21
	Sextet A (Octa)	0.388±0.026	0.053±0.023	49.66±1.36	19.55
	Sextet B (Octa)	0.378±0.015	0.026±0.016	48.36±1.59	19.35
	Sextet C (Tetra)	0.224±0.029	0.052±0.026	38.39±2.01	23.36
X=0.08	Doublet (S. P.)	0.355±0.016	0.422±0.009	-	38.73
	Sextet A (Octa)	0.384±0.026	0.052±0.009	50.36±2.22	20.31
	Sextet B (Octa)	0.341±0.056	0.046±0.012	48.22±1.18	19.45
	Sextet C (Tetra)	0.228±0.053	0.051±0.013	37.66±2.33	21.49

Journal Pre-proof

Table 12 Calculated values of isomer shift (IS), quadrupole splitting (QS) and hyperfine magnetic field for $Mn_{0.65}Zn_{0.25}Fe_{2-x}Nd_xO_4$ irradiated at 1000Gy.

Sample	Iron site spectra	Isomer shift (IS) mm/s	Quadrupole splitting (QS) mm/s	Hyperfine field (Tesla)	Relative area (%)
X=0.04	Doublet (S. P.)	0.351±0.026	0.429±0.015	-	39.21
	Sextet A (Octa)	0.386±0.015	0.056±0.018	49.96±1.13	19.55
	Sextet B (Octa)	0.337±0.019	0.049±0.021	46.32±0.98	19.34
	Sextet C (Tetra)	0.234±0.048	0.031±0.005	37.38±1.17	21.90
X=0.06	Doublet (S. P.)	0.349±0.011	0.434±0.008	-	39.43
	Sextet A (Octa)	0.388±0.024	0.037±0.025	50.23±2.36	19.55
	Sextet B (Octa)	0.346±0.011	0.046±0.011	49.46±2.52	19.35
	Sextet C (Tetra)	0.232±0.029	0.049±0.016	38.67±2.01	23.36
X=0.08	Doublet (S. P.)	0.336±0.016	0.425±0.022	-	39.77
	Sextet A (Octa)	0.385±0.066	0.048±0.018	51.23±1.25	19.86
	Sextet B (Octa)	0.342±0.026	0.053±0.011	49.55±1.11	18.69
	Sextet C (Tetra)	0.224±0.034	0.052±0.018	38.86±2.13	21.68

It may be seen that there is an increase in the relative area of the superparamagnetic doublet with an increasing γ radiation dose. This provides a clear indication of enhancement in superparamagnetic behavior which is a characteristic observed in nanomagnetic materials when the reduction of particle size reaches below a critical limit. Out of the remaining three sub-spectra, one corresponds to Fe ions occupying the tetrahedral site and the remaining two sextets correspond to the octahedral Fe ion sites. The isomer shift (IS), quadrupole splitting (QS), and hyperfine field (H_{hf}) were calculated from the fitting of spectra. By comparing the values in Tables 10, 11, and 12 with published data we can conclude that the Fe exists at both the octahedral and the tetrahedral site as Fe^{+3} that too in the high spin state.

The hyperfine field at B site increases with increasing gamma radiation dose. This enhancement in the hyperfine field can be attributed to the lowering of Fe^{+2}/Fe^{+3} ratios due to the increase of Fe^{+3} ions in the high spin state. The hyperfine field at the A-site was found to increase marginally due to the transfer of Fe^{+3} at the tetrahedral site as a consequence of gamma radiation exposure. An increase in the relative area of the paramagnetic doublet with increasing gamma radiation dose at the expense of the relative area of magnetic sextets indicates the enhancement in superparamagnetic behavior which can be attributed to the reduction of particle size as a result of gamma radiation exposure [33-41].

4. Conclusion

Nanocrystalline rare earth doped manganese zinc ferrite nanomaterials with composition $Mn_{0.65}Zn_{0.35}Fe_{2-x}Nd_xO_4$ (x = 0.04, 0.06 and 0.08) were successfully prepared using combustion method. Samples were observed to crystallize in the cubic spinal structure. These samples were exposed to three different doses (500Gy, 750Gy and 1000Gy) of gamma radiation. The lattice constant of the samples was first observed to increase with increasing Nd^{+3} concentrations due to the inclusion of Nd^{+3} ions at the octahedral site and a proportionate increase was seen further with increasing gamma radiation dose with an average increase of 1.2% for maximum gamma radiation dose. This enhancement was attributed to an increase in the concentration of Fe^{+3} in high spin state at both the tetrahedral and the octahedral sites. Other structural parameters like crystallite size and mass density were seen to decrease with increasing gamma radiation dose and were explained on the bases of the strain-based model. A remarkable average crystallite size reduction of approximately 60% was seen for all the samples with increasing gamma radiation dose. The percentage porosity of the samples was seen to increase with increasing gamma radiation dose. The saturation magnetization of as-prepared samples showed an increasing trend with increasing Nd^{+3} concentrations and showed additional enhancement proportional to the gamma radiation dose attaining 20 % increase in saturation magnetization in all the samples irradiated with 1000Gy. The magnetization of as-prepared and gamma irradiated samples was seen to increase with decreasing temperature with a narrow distribution blocking temperature ranges. Mossbauer spectra confirmed the existence and enhanced dominance of Fe^{+3} ions in the high spin state along with increase in number of particles exhibiting superparamagnetic behaviour.

References

1. D. W. Hopkins, A Reaction Between Solids; The Formation of Zinc Ferrite from Zinc Oxide and Ferric Oxide, J. Electrochem. Soc. 96(3), (1949) 195-203.
2. Xuning Li, Zhaohui Wang, Bo Zhang, Alexandre I. Rykov, Mamdouh A. Ahmed, Junhu Wang, Fe x Co 3−x O 4 nanocages derived from nanoscale metal-organic frameworks for removal of bisphenol A by activation of peroxymonosulfate, Applied Catalysis B: Environmental, 181 (2016) 788–799.
3. R. Arulmurugan, G. Vaidyanathan, S. Sendhilnathan, B. Jeyadevan, Mn–Zn ferrite nanoparticles for ferrofluid preparation: Study on thermal–magnetic propertiesJournal of Magnetism and Magnetic Materials 298 (2006) 83–94.

Journal Pre-proof

4. Ferrite-based magnetic nanofluids used in hyperthermia applications, Ibrahim Sharifi, H. Shokrollahi, S. Amiri, Journal of Magnetism and Magnetic Materials 324 (2012) 903–915.
5. M. Mahmoudi, S. Sant, B. Wang, S. Laurent, T. Sen, Superparamagnetic iron oxidenanoparticles (SPIONs): development, surface modification, and applications in chemotherapy, Advanced Drug Delivery Reviews, 63 (2010) 24–46.
6. H. Mohseni, H. Shokrollahi, Ibrahim Sharifi, Kh. Gheisari, Magnetic and structural studies of the Mn-doped Mg–Zn ferrite nanoparticles synthesized by the glycine nitrate process, Journal of Magnetism and Magnetic Materials, 324 (2012) 3741–3747.
7. Pranav P. Naik, R. B. Tangsali, Enduring Effect of Rare Earth (Nd +3) Doping and Radiation on Electrical properties of Nanoparticle Manganese Zinc Ferrite, Journal of Alloys and Compounds, 723 (2017) 266-275.
8. Pranav P. Naik, R. B. Tangsali, S. S. Meena, Influence of Rare Earth (Nd +3) Doping on Structural and Magnetic Properties of Nanocrystalline Manganese-Zinc Ferrite, Materials Chemistry and Physics, 191 (2017) 215-224.
9. Pranav P. Naik, R. B. Tangsali, B. Sonaye, S. Sugur, Gamma radiation stimulated unwavering structural and magnetic refinements in Mn x Zn 1-x Fe 2 O 4 nanoparticles, Advanced Science Letters, 22 (2016) 752-758.
10. Pranav P. Naik, R. B. Tangsali, B. Sonaye, and S. Sugur, Sustained Augmentation in Electrical properties of Mn x Zn 1-x Fe 2 O 4 nanoparticle s provoked by High Energy Gamma Radiation, J. Nano. Adv. Mat. 3(1), (2015) 1-7.
11. Pranav P. Naik, R. B. Tangsali, B. Sonaye, S. Sugur, Radiation-induced structural and magnetic transformations in nano-particle Mn x Zn (1-x) Fe 2 O 4 ferrites, Journal of Magnetism and Magnetic Materials, 385, (2015) 377–385.
12. P. P. Naik, R. B. Tangsali, S. S. Meena, Pramod Bhatt, B. Sonaye, S. Sugur, Gamma Radiation Roused Lattice Contraction effects investigated by Mössbauer spectroscopy in nanoparticle Mn-Zn Ferrite, Radiation Physics and Chemistry, (2014) 147–152.
13. P. P. Naik, R. B. Tangsali, S. S. Meena, Pramod Bhatt, B. Sonaye, S. Sugur, Radiation stimulated permanent alterations in Structural and Electrical properties of core-shell Mn- Zn Ferrite Nanoparticles, Journal of Nano Research, 24 (2013), 194-202.
14. P. P. Naik, R. B. Tangsali, B. Sonaye, and S. Sugur, Enrichment of magnetic alignment stimulated by γ-radiation in core-shell type nanoparticle Mn-Zn ferrite, AIP Conf. Proc. 1512, (2013) 354.
15. I. M. Hamada, X-ray diffraction and IR absorption in the system Co 0.6 Zn 0.4 MnxFe 2-x O 4 before and after γ-irradiation, J. Magn. Magn. Mater. 271, (2004) 318–325.

Journal Pre-proof

16. H. E. Hassan, T. Sharshar, M. M. Hessien, O. M. Hemeda, Effect of γ-rays irradiation on Mn–Ni ferrites structure, magnetic properties, and positron annihilation studies, Nucl.Instrum.MethodsPhys.Res. B 304, (2013) 72–79.
17. L. Ben Tahar, L. S. Smiri, M. Artus, A.-L. Joudrier, F. Herbst, M.J. Vaulay, S. Ammar, F. Fievet, Characterization and magnetic properties of Sm- and Gd-substituted CoFe2O4 nanoparticles prepared by forced hydrolysis in polyol, Materials Research Bulletin 42, (2007) 1888–1896.
18. N. Rezlescu, E. Rezlescu, The influence of Fe substitutions by R ions in a Ni Zn Ferrite, Solid State Commun. 88 (2) (1993) 139.
19. M. Veena, G.J. Shankaramurthy, H.S. Jayanna, H.M. Somashekarappa,Effect of γ- rays irradiation on structural, electrical and magnetic properties of Dy3+ substituted nanocrystalline Ni-Zn ferrites, Journal of Alloys and Compounds,Volume 735, 2018, Pages 2532-2543,
20. Santosh Kalunge, Ashok V. Humbe, Mangesh V. Khedkar, S. D. More, A. P. Keche and A. A. Pandit, Investigation on Synthesis, Structural and Electrical properties of Zinc Ferrite on Gamma Irradiation, Journal of Physics: Conference Series, Volume 1644, International Web Conference on Advanced Material Science and Nanotechnology (NANOMAT -2020) 20-21 June 2020, Nandgaon Khandeshwar India
21. Pooja Sarker, Sapan Kumar Sen, M.N.H. Mia, M.F. Pervez, A.A. Mortuza, Sazzad Hossain, M.F. Mortuza, M.H. Ali, Salahuddin Nur, Humayun Kabir, M.A.M. Chowdhury, Effect of gamma irradiation on structural, morphological and optical properties of thermal spray pyrolysis deposited CuO thin film, Ceramics International, Volume 47, Issue 3, 2021, Pages 3626-3633
22. Routray KL, Sanyal D, Behera D, Gamma irradiation induced structural, electrical, magnetic and ferroelectric transformation in bismuth-doped nanosized cobalt ferrite for various applications, *Materials Research Bulletin* (2018), https://doi.org/10.1016/j.materresbull.2018.10.019
23. N. Okasha, S.I. El Dek, M.K. Abdelmaksoud, D.N. Ghaffar, Enhanced structure and magnetic properties of doped nanomagnetite by γ-irradiation, Journal of Alloys and compounds (2018), doi: 10.1016/j.jallcom.2017.12.050
24. G. L. Sun, J. B. Li, J. J. Sun, and X.-Z. Yang, The influences of Zn2+ and some rare-earth ions on the magnetic properties of nickel-zinc ferrites, J. Magn. Magn. Mater. 281 (2004) 173.

25. K. Rama Krishna, K. Vijaya Kumar, Dachepalli Ravinder, Structural and Electrical Conductivity Studies in Nickel-Zinc Ferrite, Advances in Materials Physics and Chemistry 2, (2012) 185-191.
26. S.M. Patange, S.E. Shirsath, G.S. Jangam, K.S. Lohar, S.S. Jadhav, K.M. Jadhav, Rietveld structure refinement, cation distribution and magnetic properties of Al 3+ substituted NiFe2O4 nanoparticles, Journal of Applied Physics, 109, (2011) 053909.
27. R. Naik, A.V. Salker, Change in the magnetostructural properties of rare earth doped cobalt ferrites relative to the magnetic anisotropy Journal of Material Chemistry, 22, (2012) 2740.
28. José M Vargas, Leandro M Socolovsky, Marcelo Knobel, Daniela Zanchet, Dipolar interaction and size effects in powder samples of colloidal iron oxide nanoparticles, Nanotechnology 16, (2005) S285-90.
29. Z.C.,XU, Magnetic anisotropy and Mössbauer spectra in disordered lithium–zinc ferrites Journal of Applied Physics, 93, (2003) 4746-4749.
30. F. Patil, M Lenglet. Solid State Communications, 86, (1993) 67–71.
31. S. K. Sharma, Ravi Kumar, V. V Siva Kumar, M Knobel, V. R. Reddy, A. Gupta, M Singh, Nuclear Instruments and Methods in Physics Research B, 248, (2006) 37–41.
32. J.P. Vejpravov, V. Sechovsk´y, WDS'05 Proceedings of Contributed Papers, Part III, (2005) 518–523.
33. K. Vasundhara, S. N. Achary, S. K Deshpande, P. D. Babu, S. S. Meena, A. K. Tyagi, Size dependent magnetic and dielectric properties of nano CoFe2O4 prepared by a salt assisted gel-combustion method J. Appl. Phys. 113, (2013) 194101.
34. S. R. Naik, A. V. Salker, S. M. Yusuf, S. S. Meena, Influence of Co2+ distribution and spin–orbit coupling on the resultant magnetic properties of spinel cobalt ferrite nanocrystals J. Alloys Compd. 566, (2013) 54–61.
35. Shalendra Kumar et al, Mössbauer studies of Co0.5CdxFe2.5−xO4 (0.0⩽x⩽0.5) ferrite
, Physica B, 403, (2008) 3604–3607.
36. D. E. Dickson, F. J. Berry, Mossbauer Spectroscopy. Cambridge University Press, London,1986, 22.
37. S.S. Shinde, Sher Singh Meena, S.M. Yusuf, K.Y. Rajpure, M€ossbauer, Raman, and magnetoresistance study of aluminum-based iron oxide thin films, J. Phys. Chem. C 115 (2011) 3731-3736.
38. M.M. Eltabeya, W.R. Agami, H.T. Mohsen, Improvement of the magnetic properties for Mn-Ni-Zn ferrites by rare earth Nd +3 ion substitution, J. Adv. Res. 5, (2014) 601-605.

Journal Pre-proof

39. L. Zhao, H. Yang, X. Zhao, L. Yu, Y. Cui, S. Feng, Magnetic properties of CoFe2O4 ferrite doped with rare earth ion Material Letters 60, (2006)1-6.
40. D.S. Mathew, R.-S. Juang, An overview of the structure and magnetism of spinel ferrite nanoparticles and their synthesis in microemulsions ,Chemical Engineering Journal 129, (2007)51–65.
41. A. Kale, S. Gubbala, R. Misra, Magnetic behavior of nanocrystalline nickel ferrite synthesized by the reverse micelle technique Journal of Magnetism and Magnetic Materials 277, (2004) 350–358.

Journal Pre-proof

Journal Pre-proof

Highlights

1. Preparation of Nd^{+3} doped Mn-Zn ferrite nanoparticles employing the combustion method.
2. Successful irradiation of nanoparticles with gamma radiation.
3. Particle reduction explained on the bases strain-based model.
4. Enhanced dominance of Fe^{+3} in high spin state at both A-Site and B-site
5. Enhanced saturation magnetization due to gamma exposure

Journal Pre-proof

Journal Pre-proof

The manuscript entitled “Effect of Gamma Radiation on Structural and Magnetic properties of Rare Earth Doped Manganese Zinc Ferrite Nanoparticles” is a joint effort of all the following authors.

Dr. Pranav P. Naik (The corresponding author) did the experimental work, manuscript preparation and data analysis.

Dr. Rahul Singhal played an important role in material synthesis and structural data analysis. Dr. Diptesh Naik was involved in interpreting the radiation effect on structural and morphological properties of the material

Mr. Sher Singh Meena and Dr. Pramod Bhatt contributed through magnetic measurements and Mossbauer data analysis.

Journal Pre-proof

Journal Pre-proof

Declaration of interests

☒ The authors declare that they have no known competing financial interests or personal relationships that could have appeared to influence the work reported in this paper.

☐The authors declare the following financial interests/personal relationships which may be considered as potential competing interests:

Journal Pre-proof